Con ... --32

58930-00-105

ANL/CP--76267

DE92 016192

JUN 24 1992

MANUSCRIPT

GRAIN BOUNDARY WEAK LINKS IN HIGH-T_c SUPERCONDUCTORS*

Donglu Shi, S. Sengupta, K.C. Goretta, S. Salem-Sugui, Jr.

Materials Science Division and Materials & Components Technology Division
Argonne National Laboratory, Argonne, IL 60439

M. Smith and Y.N. Lwin

Western Illinois University, Macomb, IL 61455

INVITED paper for Proceedings of 1992 Spring Meeting of the Materials Research Society, San Francisco, CA, April 27-May 1, 1992

jmc

*Work supported by the U.S. Department of Energy, BES-Materials Sciences and Conservation and Renewable Energy as part of a DOE program to develop Electric Power Technology, under contract #W-31-109-ENG-38.

GRAIN BOUNDARY WEAK LINKS IN HIGH-T_c SUPERCONDUCTORS

DONGLU SHI,* S. SENGUPTA,* K. C. GORETTA,* S. SALEM-SUGUI, JR.,* M. SMITH,** and Y. N. LWIN**
*Argonne National Laboratory, Argonne, IL 60439
**Department of Physics, Western Illinois University, Macomb, IL 61455

ABSTRACT

The transport critical current density (J_c) for high-T_c thin films, bicrystals, and bulk ceramics is shown to be determined by magnetic field penetration into the grain boundaries. The gross grain orientations may not in all cases be an important factor in determining this penetration. The parameter $(\lambda_G/\lambda_J)^2$ can characterize the strength of the grain boundary coupling, which depends mainly on the crystal coherence and connectivity at the boundary area.

INTRODUCTION

The grain boundaries in bulk high-T_c superconductors generally exhibit weak-link effects, in large part as a result of short coherence lengths. These weak links severely limit the transport critical current density (J_c), even at low magnetic fields [1-3]. Dimos et al. [4] developed a method to study the angular dependence of the critical current density across grain boundaries (J_{gb}) of bicrystalline epitaxial $YBa_2Cu_3O_x$ (123) thin films on $SrTiO_3$ bicrystals. The grains of the films were oriented at various angles (θ) to each other. They found that at 4.2 K the ratio J_{gb}/J_g, where J_g was the J_c measured within a single grain, was reduced 50 times as θ increased from 0° to 35°. Based on these results, they concluded that the strong angular dependence of J_{gb} was associated with the distortion of vortices by grain boundary dislocations. Their conclusions implied that high-T_c superconductors with high-angle grain boundaries would not be capable of producing high transport J_c values.

In contrast, Babcock et al. [5] reported that weak-link behavior was not observed in bicrystals with high-angle grain boundaries. J_{gb} values of bicrystals with θ = 3°, 14°, 22°, 38°, and 90° were obtained in fields up to 7 T. All of the crystals appeared to exhibit J_c behavior that was controlled by flux pinning (i.e., weak-link effects were not observed). These data indicate that high-angle grain boundaries may not necessarily be connected with Josephson junction weak links. The J_c values of the individual grains of the bicrystals were low, however, and thus this conclusion is not fully established.

In this paper, the nature of the Josephson junction [6] is used to explain the flux-pinning-dominated and weak-link-dominated transport J_c in 123 samples that contain high-angle grain boundaries.

BACKGROUND

One can assume that each grain boundary in 123 is a Josephson junction of length, L, of the grain size and thickness, t. The coupling strength, F, of each grain boundary is related by the ratio of the penetration depth in the grain, λ_G, to the Josephson penetration depth,λ_J, by $F = (\lambda_G/\lambda_J)^2$ [7]. In the strong-coupling limit [3], the expression can be written as $F = (\lambda_G/\lambda_J)^2 = J_{gb}/J_g$, and thus one can see that grain boundaries exhibit weak coupling when $(\lambda_G/\lambda_J)^2 << 1$.

The occurrence of a Josephson junction is dependent only on the ratio of the London penetration depth to the Josephson penetration depth. If the the grain boundary is weakly coupled, as has been observed for conventionally sintered samples, the boundary area is uniformly penetrated by the applied field, and $(\lambda_G/\lambda_J)^2 << 1$. If the grain boundary is strongly coupled, as is often the case for melt-textured bars or flux-grown bicrystals, the high crystal coherency at the boundary makes it difficult for the field to penetrate the boundary. Thus, $(\lambda_G/\lambda_J)^2$ would approach or exceed 1 for this type of grain boundary. The coupling strength has to do not only with grain orientation, but also with the nature of the boundary itself. For example, weak-link effects have been observed in magnetically aligned samples with low-angle boundaries. Although high-T_c superconductors are highly anisotropic, the current will redistribute across high-angle grain boundaries if they are strongly coupled. On the other hand, weak-link behavior can still exist at low-angle grain boundaries if they are weakly coupled. The transport J_c will be severely reduced only when the grain boundaries are penetrated by an applied field.

It has been reported that transport J_c exhibits flux-pinning-dominated behavior in melt-processed samples [8]. Although these materials contain mainly low-angle grain boundaries [8], substantial amounts of high-angle grain boundaries have been observed in these samples, which may provide evidence for strongly-coupled high-angle grain boundaries in these materials. The materials discussed in these studies were produced by techniques that have been described [1,8-10]. Bulk 123 specimens were produced by sintering cold-pressed compacts in O_2 at temperatures from 885 to 1050°C. Melt-processed bars were produced by cooling in air from 1050°C at ≈1°C/min. The melt-processed bars contained large regions of well-aligned grains, but also regions with large misorientations. These bars had transport J_c values of ≈4.4 x 10^4 A/cm^2 at 77 K in fields greater than 1 T [9]. Representative microstructures are shown in Fig. 1. J_c values characteristic of these microstructures are shown in Fig. 2.

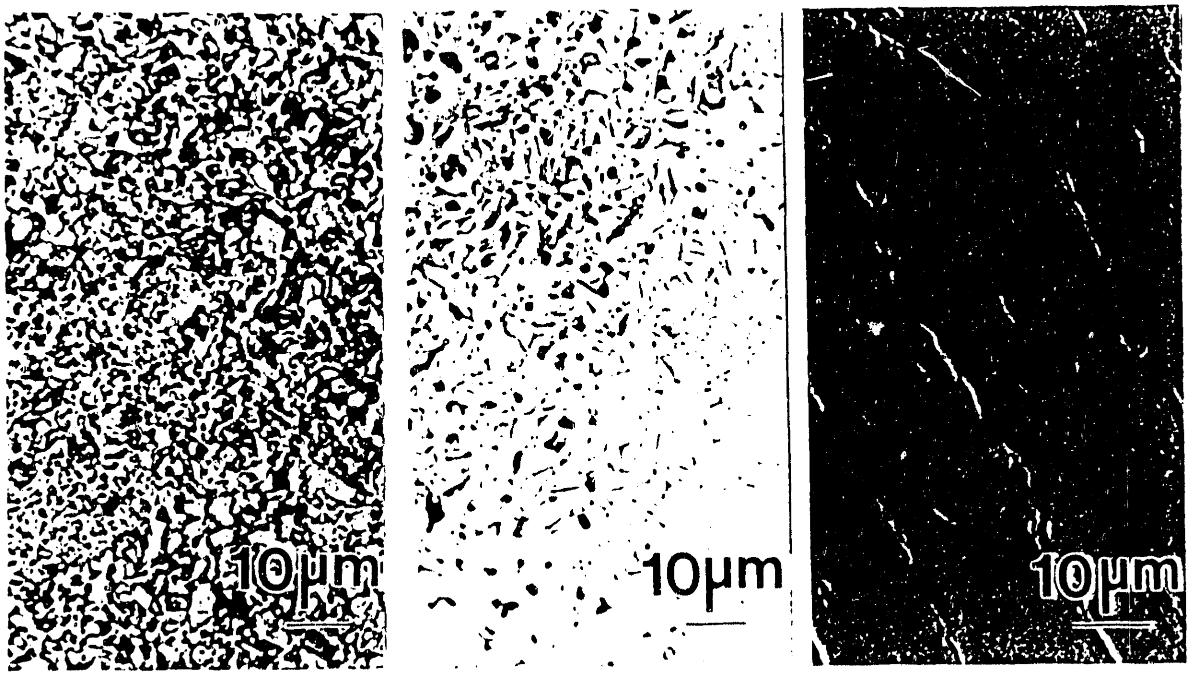

Fig. 1. Microstructures of 123: (a) porous compact sintered at 885°C, (b) dense compact sintered at 1000°C [1], and (c) elongated grains in melt-textured 123 [8,10].

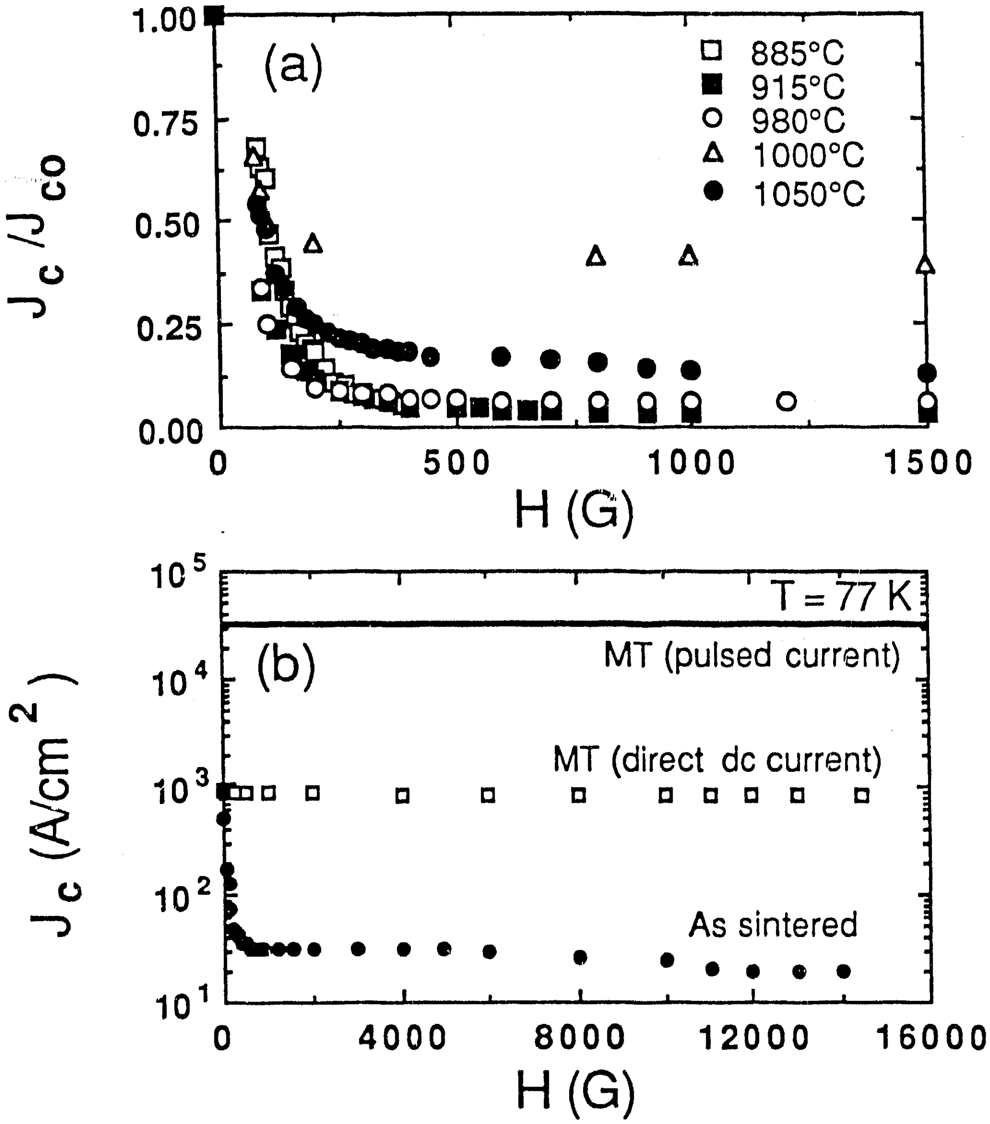

Fig. 2. J_c data for (a) 123 sintered at the temperatures shown [1] and (b) sintered vs. melt–textured 123 [10].

DISCUSSION

Although microscopy data have not indicated the essential structural differences between strongly and weakly coupled grain boundaries, certain possibilities can be ruled out in terms of the formation of grain boundaries through different processing methods. Grain boundaries must be treated differently for liquid–processed and solid–state–sintered samples. It is reasonable to consider high–angle grain boundaries to be of the following three types [11]: (1) amorphous layer present (AGB); (2) transition structure (TGB); and (3) perfect grains up to the boundary (PGB), as for a coincident–site lattice. When there exists a layer with no well–defined lattice structure with relation to the grains, the properties of the boundary will be largely independent of the orientation, and the boundary may be considered as AGB. However, if the grain boundary is structurally related to the adjacent grains and the properties of the layer depend on the difference of the orientation, TGB may be an appropriate term to describe the boundary. The term PGB describes the distinct interface between two perfect crystals with negligible structural distortion at the edges of the crystals.

Amorphous-type or highly disordered grain boundaries are likely to be formed in sintered samples. Bulk samples are formed through diffusional processes at temperatures of ≈850–1000°C. Sintering by solid-state diffusion is slow, and grains have little chance to reorient into low-energy configurations. In addition, second phases and pores can be present. The grain boundaries may possess a high degree of disorder and be glassy in nature. This type of boundary can be penetrated easily by an applied field, even for low-angle boundaries, and thus, $F << 1$.

In contrast, grains are formed fundamentally differently in melt-texturing [9-14]. Diffusion is rapid in a liquid. In addition, the duration of the growth process is typically significantly longer (in our studies, liquids were present for 3–5 days) than is a conventional sintering time (less than 1 day). Therefore, in melt-processing, the grain boundaries can migrate and are more likely to assume low-energy configurations. Low-angle and low-energy boundaries are preferred, and texturing in large regions results. These grain boundaries tend to be types PGB and TGB [15].

Transmission electron microscopy has been performed on many specimens. Films and melt-textured bars often exhibited substantial misorientation, but with much faceting of the grain boundaries, whereas the sintered specimens exhibited no facets on the high-angle boundaries. Most grain boundaries in the melt-textured bars were of the low-angle type. It is noted that the high-resolution images of the boundaries in the films and melt-textured bars indicated high coherence between the grains [16]. The crystal coherence and connectivity at grain boundaries, including high-angle boundaries, were generally much higher for the melt-processed materials than for sintered materials. The high crystal coherency may have been achieved by a facet structure or by the gross orientations of the grains themselves. These types of grain boundaries are strongly coupled and thus are not easily penetrated by an applied field. As shown in Fig. 2, if even some liquid was present during heat treating (e.g., sintering at 1000°C), the J_c degraded more slowly in an applied field than it did for solid-state-processed 123. The presence of a liquid phase seems to have allowed for better coupling of the grains. The data in Fig. 2 are related schematically in Fig. 3 to the dominant grain boundary features.

The degree of field penetration into grain boundaries has been examined by magnetization measurements. It has been shown [17] that the peak positions in the flux-creep-rate (dM/dlnt) vs. field (or temperature) plots correspond to the full penetration field (H*). Sintered 123 samples have exhibited considerably lower H* values than melt-textured samples [17]. It is clear that H* is closely related to the field penetration at weakly linked areas and that H* can serve as an indirect measure of the coupling parameter, F. As calculated by Hylton and Beasley [7], F = 0.00063 and 8.6 for a ceramic and a single-crystal 123, respectively. Magnetization measurements provide strong evidence for the difference of field penetration in weakly and strongly coupled samples, which indicates that the coupling strength is related to the connectivity of the crystals. The observations to date suggest that faceting of the grain boundaries of melt-textured samples may be a mechanism by which highly coherent boundaries are formed, even for high-angle boundaries.

CONCLUSION

Transport J_c in a high-T_c superconductor such as 123 is significantly reduced only when the grain boundaries are penetrated by a magnetic field and $(\lambda_G/\lambda_J)^2 << 1$. The degree to which a boundary area is penetrated by an applied field is related to the crystal coherence and connectivity at the boundary area. For 123, melt-processing was found to produce high J_c values and to promote well-connected grains, either through formation of low-angle boundaries or grain boundary facets.

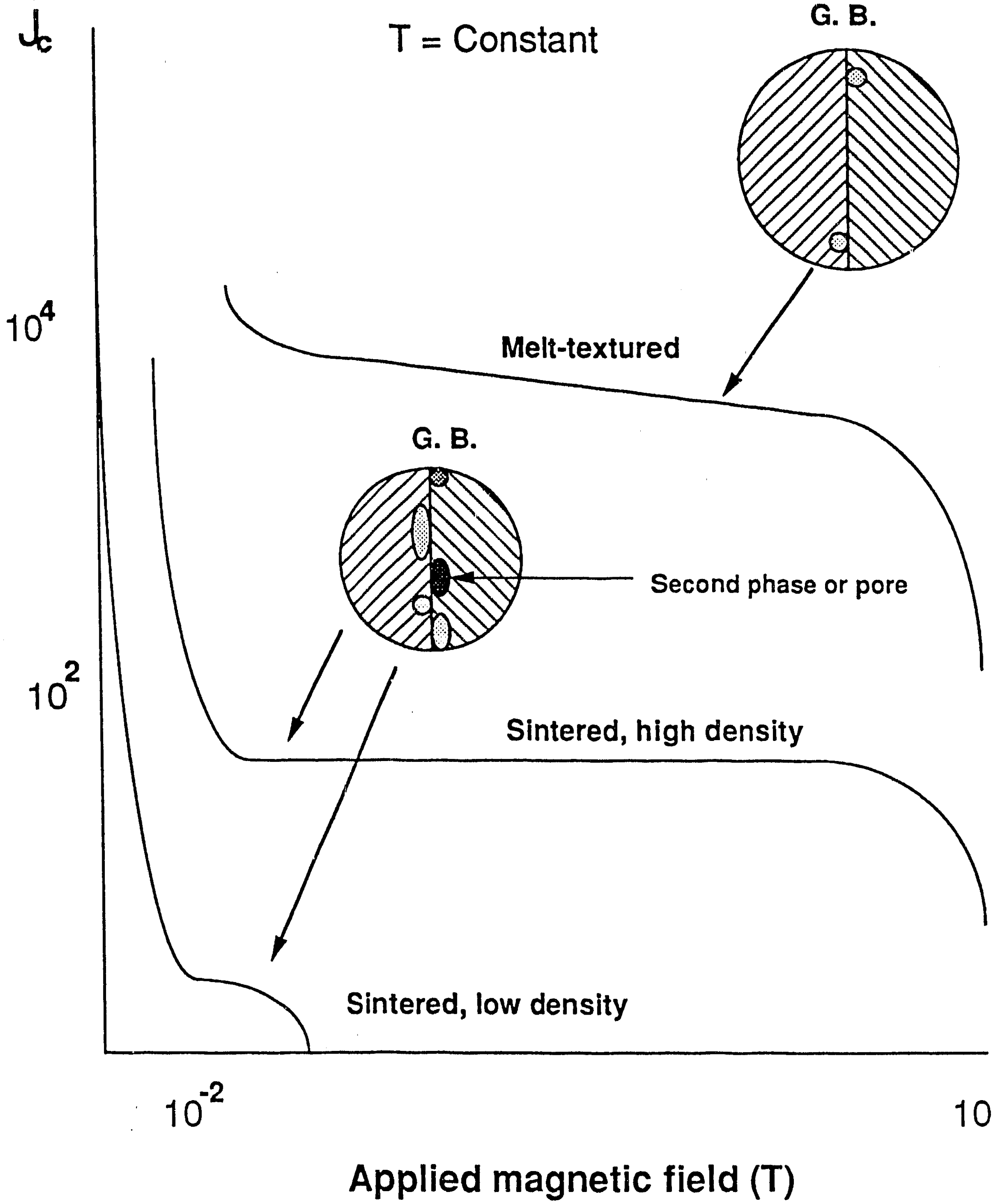

Fig. 3. Schematic illustration of J_c data and related grain boundary microstructures. Note that the transport J_c is proportional the area of strongly coupled regions at grain boundaries in the sintered samples. As more and more liquid phase is induced during sintering, the area of strongly coupled regions significantly increases. Thus, as an extreme case, most of the grains are strongly coupled in the melt-processed samples.

ACKNOWLEDGMENT

This work was supported by the U.S. Department of Energy, Basic Energy Sciences–Materials Sciences, under Contract W-31-109-Eng-38

REFERENCES

1. D. Shi, D. W. Capone II, G. T. Goudey, J. P. Singh, N. J. Zaluzec, and K. C. Goretta, Mater. Lett. 6, 217 (1988).
1. R. L. Peterson and J. W. Ekin, Physica C 157, 325 (1989).
2. R. B. Stephens, Cryogenics 29, 399 (1989).
3. D. Shi, J. G. Chen, M. Xu, A. L. Cornelius, U. Balachandran, and K. C. Goretta, Supercond. Sci. Technol. 3, 222 (1990).
4. D. Dimos, P. Chaudhari, J. Mannhart, and F. K. LeGoues, Phys. Rev. Lett. 61, 219 (1988).
5. S. E. Babcock, X. Y. Cai, D. L. Kaiser, and D. C. Larbalestier, Nature 347, 167 (1990).
6. T. Van Duzer and C. W. Turner, "Principles of Superconductive Devices and Circuits" (Elsevier North Holland, Amsterdam, 1981) p. 139.
7. T. L. Hylton and M. R. Beasley, Phys. Rev. B. 39, 9042 (1989).
8. D. Shi, H. Krishnan, J. M. Hong, D. Miller, P. J. McGinn, W. H. Chen, M. Xu, J. G. Chen, M. M. Fang, U. Welp, M. T. Lanagan, K. C. Goretta, J. T. Dusek, J. J. Picciolo, and U. Balachandran, J. Appl. Phys. 68, 228 (1990).
9. D. Shi, J. G. Chen, M. Xu, A. L. Cornelius, U. Balachandran, and K. C. Goretta, Supercond. Sci. Technol. 3, 222 (1990).
10. D. Shi, M. M. Fang, J. Akujieze, M. Xu, J. G. Chen, and C. Segre, Appl. Phys. Lett. 57, 2606 (1990).
11. P. G. Shewmon, in "Physical Metallurgy," ed. B. Chalmers (John Wiley and Sons, New York, 1959) p. 110.
12. M. Murakami, M. Morita, and N. Koyama, Jpn. J. Appl. Phys. 28, L1754 (1989).
13. S. Jin, T. H. Tiefel, R. C. Sherwood, M. E. Davis, R. B. Van Dover, G. W. Kammlott, R. A. Fastnacht, and H. D. Keith, Appl. Phys. Lett. 52, 2074 (1988).
14. P. J. McGinn, M. Black, and A. Valenzuela, Physica C 156, 57 (1988).
15. Y. Zhu, H. Zhang, H. Wang, and M. Suenaga, preprint (1991).
16. Y. Gao, G. Bai, D. J. Lam, and K. L. Merkle, Physica C 173, 487 (1991).
17. D. Shi, M. Xu, A. Umezawa, and R. F. Fox, Phys. Rev. B 42, 2062 (1990).

DATE FILMED

8/04/92